PriMera Scientific Engineering
Volume 7 Issue 3 September 2025
ISSN: 2834-2550

PriMera Scientific Publications

Tailoring the Mechanical and Microstructural Properties of Ti-Zr-Based Carbide Composites via Spark Plasma Sintering: Impact of Molybdenum and Tungsten Additions

Type: Research Article
Received: August 01, 2025
Published: September 03, 2025

Citation:
Badis Bendjemil., et al. "Tailoring the Mechanical and Microstructural Properties of Ti-Zr-Based Carbide Composites via Spark Plasma Sintering: Impact of Molybdenum and Tungsten Additions". PriMera Scientific Engineering 7.3 (2025): 13-21.

Badis Bendjemil[1]*, Lassaad Ajilil[2], Khaoula Safi[1], Sinda Sassi[2], Mounir Ferhi[2] and Karima Horchani Naifer[2]

[1]Laboratory of applied mechanic and novel nanomaterials, University of 08 May 1945 Guelma, avenue 19 May 1956, CS 401, 24000 Guelma, Algeria

[2]Physical Chemistry Laboratory for Mineral Materials and their Applications, National Center for Research in Materials Sciences CNRSM, Technopole Borj Cedria, Tunisia

***Corresponding Author:** Badis Bendjemil, Laboratory of applied mechanic and novel nanomaterials, University of 08 May 1945 Guelma, avenue 19 May 1956, CS 401, 24000 Guelma, Algeria.

Abstract

This study aims to explore the microstructural and compositional evolution of Ti/Zr-based carbide composites fabricated via Spark Plasma Sintering (SPS), focusing on the effects of molybdenum (Mo) and tungsten (W) doping. Binary (Ti-C, Zr-C), ternary (Ti-Zr-C), and quaternary (Ti-Zr-C-Mo, Ti-Zr-C-W) systems were synthesized and characterized using X-ray diffraction (XRD), scanning electron microscopy (SEM), and energy-dispersive X-ray spectroscopy (EDS). XRD analysis confirmed the formation of face-centered cubic (FCC) NaCl-type carbide phases and progressive solid solution formation upon dopant incorporation. SEM revealed that Mo doping promotes submicron grain refinement and full densification, while W doping induces the in situ formation of WC nanoparticles, enhancing matrix cohesion and hardness. EDS confirmed homogeneous elemental distributions and successful dopant integration without significant oxidation. The undoped Ti-Zr-C composite exhibited phase separation beneficial for crack deflection but showed grain size heterogeneity. Overall, Mo and W offer complementary mechanisms for improving the microstructure and mechanical properties of Ti/Zr-based carbide composites. These findings provide a foundation for the design of next-generation ceramic materials tailored for cutting tools and ballistic protection applications.

Keywords: TiC-ZrC composites; Field Assisted Spark Plasma Sintering (FAST-SPS); Carbon nanotubes (CNTs); Nano-tungsten carbide (NWC); Finale microstructure; Mechanical properties; Ballistic performance

Introduction

Transition metal carbides, particularly TiC-ZrC composites [1, 2], have emerged as promising candidates for advanced structural applications such as ballistic armor and cutting tools due to their exceptional hardness, wear resistance, and thermal stability [3-5]. However, their practical implementation faces significant challenges stemming from inherent brittleness and limited fracture toughness, which severely restrict their performance under dynamic loading conditions [3-5].

To overcome these limitations, recent research has focused on strategic doping with secondary phases including tungsten (W), molybdenum (Mo), and tungsten carbide (WC), aiming to synergistically enhance both microstructure and mechanical properties [6-10]. While previous studies have demonstrated that ZrC addition improves fracture toughness through crack deflection mechanisms [5, 11, 12], and that it can increase toughness by approximately 30% [11], these improvements often come at the cost of reduced densification [11].

Furthermore, although WC and Mo are known to refine grain structure and enhance hardness through solid-solution strengthening [7, 10, 13], there remains a critical lack of understanding regarding their combined effects with in TiC-ZrC systems. This knowledge gap is particularly evident in the context of spark plasma sintering (SPS) process optimization and the correlation between microstructural evolution and dynamic mechanical performance [2, 14, 15].

The present study addresses these shortcomings by systematically investigating the individual and combined effects of W, Mo, and WC dopants on the microstructure, mechanical properties, and densification behavior of TiC-ZrC composites fabricated via standard SPS technique [2, 7-9, 13]. Special emphasis is placed on elucidating the synergistic mechanisms between WC and , which preliminary results suggest can simultaneously improve hardness and toughness while maintaining exceptional densification (>98% relative density) [16, 17, 18]. By combining advanced characterization techniques with ballistic performance modeling, this work provides new insights into the design of impact-resistant ceramic composites and establishes fundamental process-structure-property relationships for armor applications. The findings not only fill critical gaps in the understanding of multi-dopant systems but also pave the way for the development of next-generation protective materials with tailored mechanical properties.

Materials and Methods

Figure 1 presents the typical sintering cycle employed in this study, performed using Spark Plasma Sintering (SPS) [19]. The curves illustrate the evolution of temperature (measured by thermocouple), applied force, punch displacement rate, and total displacement as a function of time.

The figure shows an initial rapid heating ramp, during which the temperature reaches approximately 1000 °C in less than 7 minutes. Simultaneously, a compressive force of about 8 kN is applied. This stage aims to achieve pre-compaction of the powder before the activation of diffusion mechanisms.

The first thermal plateau, maintained at around 600 °C, is likely intended to thermally stabilize the sample and facilitate the release of trapped gases or impurities. During this stage, the punch speed becomes nearly zero, indicating the absence of significant displacement.

A second heating ramp leads to the main sintering plateau, held at approximately 1000 °C. This plateau, sustained for several minutes under constant load, promotes densification of the material through solid-state diffusion. The stagnation in displacement during this phase suggests that consolidation is predominantly governed by diffusive processes rather than mechanical movement.

The cycle concludes with a gradual cooling phase, combined with a controlled reduction in applied force. A slight punch displacement may be observed toward the end of the cycle, indicative of thermal shrinkage or the relaxation of internal stresses.

This SPS protocol clearly demonstrates the advantages of the technique: rapid heating, precise control [19] of thermomechanical parameters, short cycle duration, and favorable conditions for producing dense materials with fine microstructures. This approach is particularly well-suited for shaping advanced ceramics, composites, or high-performance refractory alloys [2, 13, 15].

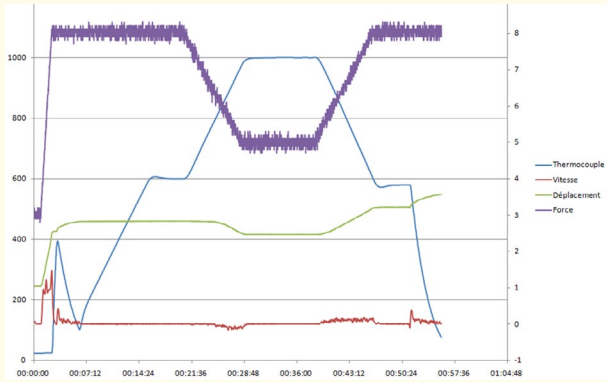

Figure 1: Typical SPS sintering cycle: evolution of temperature (blue), applied force (purple), total displacement (green), and punch speed (red) over time. The cycle includes two heating ramps, two isothermal holds, and a controlled cooling phase.

Results and Discussion

Structural Analysis

The phase structure and crystallinity of the synthesized carbide systems were investigated using X-ray diffraction (XRD). Figure 2 presents the diffraction patterns of pure binary carbides (Ti-C and Zr-C), ternary (Ti-Zr-C), and quaternary systems incorporating transition metals (Mo and W), namely Ti-Zr-C-Mo and Ti-Zr-C-W. All detected reflections can be indexed to the face centered cubic (FCC) NaCl-type structure, characteristic of transition metal carbides (space group Fm-3m), confirming the formation of carbide phases [2, 13].

The Ti-C sample exhibits sharp and intense diffraction peaks located at 2θ values corresponding to the (111), (200), (220), (311), and (222) crystallographic planes of stoichiometric titanium carbide (TiC). These results are in good agreement with the ICDD reference pattern (PDF No. 00-032-1383), indicating a well-crystallized phase with minimal structural defects. Similarly, the Zr-C sample shows well-defined peaks, shifted slightly to lower angles relative to TiC, which is consistent with the larger lattice parameter of zirconium carbide (ZrC), attributed to the larger ionic radius of Zr compared to Ti. F.2

The ternary Ti-Zr-C sample displays diffraction peaks positioned between those of the TiC and ZrC phases, suggesting the formation of a solid solution ($Ti_{1-x}Zr_x$)C. The absence of peak splitting or secondary phases indicates complete substitution of Ti and Zr within the FCC lattice [12, 20]. However, a slight broadening of the peaks is observed, which may be attributed to lattice distortion induced by cationic disorder or a reduction in crystallite size.

Incorporation of a fourth element, either Mo or W, into the Ti-Zr-C matrix leads to noticeable changes in the diffraction profiles. The Ti-Zr-C-Mo sample exhibits broader and less intense peaks compared to the ternary system, which may reflect increased lattice strain, reduced crystallite size, or partial amorphization induced by Mo incorporation [15]. Additionally, minor features in the pattern suggest the possible formation of secondary Mo-based phases, such as Mo_2C, although these could not be unambiguously resolved due to overlapping reflections.

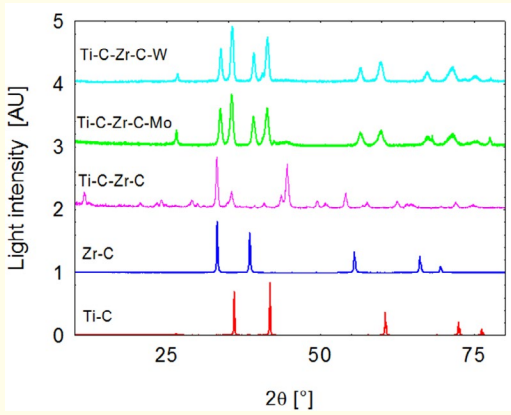

Figure 2: X-ray diffraction (XRD) patterns of synthesized carbide samples: Ti-C, Zr-C, Ti-Zr-C, Ti-Zr-C-Mo, and Ti-Zr-C-W. All major diffraction peaks correspond to the face-centered cubic (FCC) structure typical of transition metal carbides. Peak shifts and broadening in the ternary and quaternary systems indicate solid solution formation and microstructural changes due to the incorporation of Zr, Mo, and W into the TiC lattice.

For the Ti-Zr-C-W sample, the main diffraction peaks remain consistent with the FCC carbide phase, indicating that tungsten is also partially incorporated into the lattice. However, compared to the Mo-doped sample, the Ti-Zr-C-W sample exhibits narrower peaks and higher intensities, implying better crystallinity and a more homogeneous solid solution [10, 17]. The potential formation of secondary tungsten carbides (e.g., WC or W_2C) is not excluded, but their contribution appears minimal within the detection limits of the XRD setup.

Although WC phases were not clearly resolved by XRD due to their nanoscale size and low fraction, SEM and EDS analyses confirmed the presence of WC nanoparticles [16, 17].

Overall, the diffraction analysis confirms the formation of multicomponent carbide phases with a cubic structure, where Ti, Zr, Mo, and W atoms can substitute each other within the metal sublattice [2, 13]. The structural evolution observed across the series is consistent with the progressive incorporation of heavier transition metals, which influences both the lattice parameters and microstructural characteristics of the materials.

These XRD findings are in strong agreement with SEM and energy-dispersive X-ray spectroscopy (EDS) analyses. In the Ti-Zr-C composite, the clear phase separation observed in the XRD is corroborated by SEM imaging and EDS measurements, which reveal distinct Ti- and Zr-enriched regions [12, 20]. In the Ti-Zr-C-Mo system, the formation of Mo_2C detected by XRD [11, 15] explains the observed grain refinement and supports the elemental composition identified by EDS. Similarly, the WC phase identified in the Ti-Zr-C-W composite corresponds to nanoparticles observed via SEM and elevated W and C signals in EDS spectra [10, 16, 17]. Overall, the introduction of Zr, Mo, and W leads to controlled modifications in phase composition, microstructure, and crystallite size, without destabilizing the primary carbide phases. This tunability is essential for optimizing the mechanical and functional properties of advanced carbide-based composite materials.

Microstructural Analysis

SEM Morphology

The microstructural evolution of the synthesized composites was investigated via scanning electron microscopy (SEM) under con-

sistent imaging conditions (SE mode, ETD detector, accelerating voltage of 20.00 kV). As summarized in Table 1, the Ti-C composite exhibited a homogenous and well-densified microstructure, characterized by uniformly distributed TiC grains with an average size of 1-2 μm [2]. The low porosity observed in this sample reflects efficient particle bonding and densification, likely facilitated by the compatibility between Ti and carbon during SPS processing.

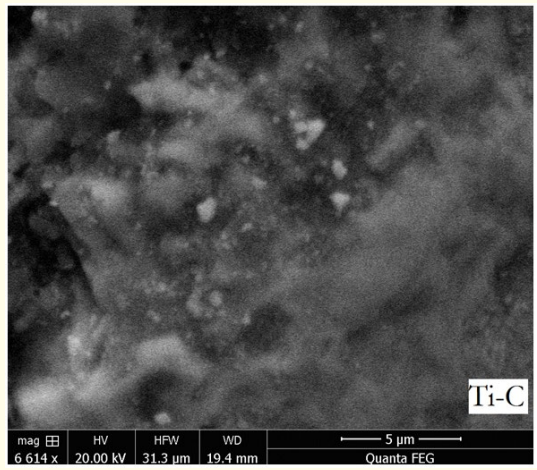

Figure 3: SEM image of the Ti-C composite at 6,614× magnification (5 μm scale bar), showing a homogeneous distribution of fine TiC grains (~1-2 μm) with minimal porosity, indicating efficient densification through SPS.

In contrast, the Zr-C composite revealed larger, angular grains averaging 2-3 μm, with moderate porosity and microstructural heterogeneity [2]. These features suggest limited sinterability of pure ZrC under identical processing conditions, possibly due to its higher-melting point and slower diffusion kinetics compared to TiC.

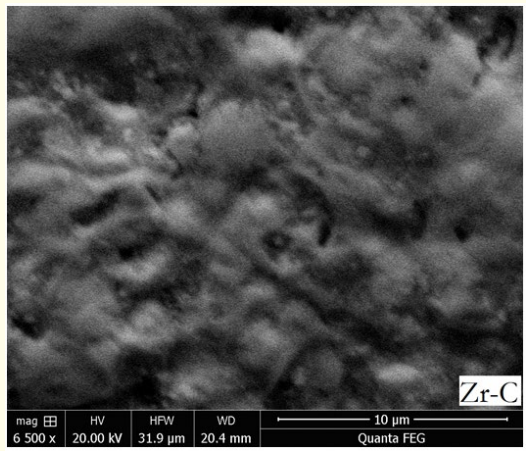

Figure 4: SEM image of the Zr-C composite at 6,500× magnification (10 μm scale bar), revealing angular ZrC grains (2-3 μm) with moderate heterogeneity and localized porosity, reflecting reduced sinterability compared to TiC.

The ternary Ti-Zr-C composite displayed distinct phase separation, with microdomains of Ti-rich (darker contrast) and Zr-rich (brighter contrast) regions. Grain sizes ranged from 1 to 4 μm. This segregation behavior is consistent with spinodal decomposition mechanisms within the (Ti,Zr)C solid solution, contributing to a heterogeneous grain morphology [12, 20]. Despite this heterogeneity, the composite showed improved densification relative to Zr-C, likely due to enhanced sintering dynamics from the presence of Ti [14].

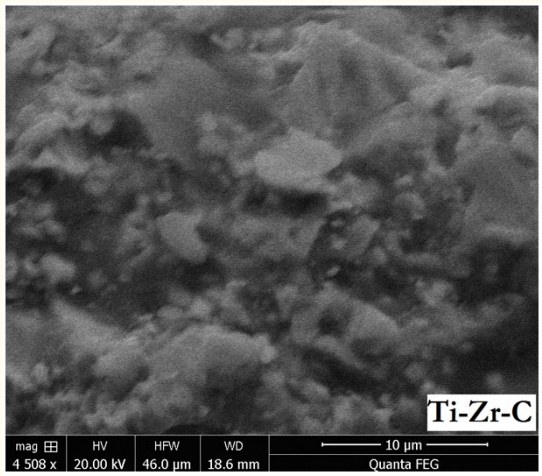

Figure 5: SEM image of the Ti-Zr-C composite at 4,508× magnification (10 μm scale bar). The microstructure displays phase separation into Ti-rich (dark) and Zr-rich (bright) regions with grain sizes ranging from 1-4 μm.

Incorporation of Mo in the Ti-Zr-C-Mo composite yielded a significantly refined microstructure. SEM images at higher magnification revealed submicron grains (<1 μm), homogeneously distributed with no visible porosity [15]. This morphology indicates that Mo acts as an effective grain growth inhibitor and promotes sintering by stabilizing grain boundaries and enhancing diffusion processes. The resulting microstructure is dense and isotropic, desirable for mechanical performance.

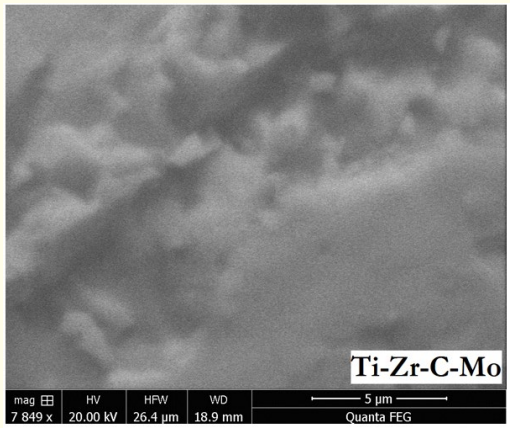

Figure 6: SEM image of the Ti-Zr-C-Mo composite at 7,849× magnification (5 μm scale bar), showing a dense, homogeneous structure composed of submicron grains (<1 μm), highlighting Mo's role in grain refinement and sintering enhancement.

The Ti-Zr-C-W composite exhibited a unique nanocomposite structure, with fine (Ti,Zr)C grains (1-2 μm) embedded with bright-contrast WC nanoparticles, uniformly dispersed across the matrix [16, 17]. The absence of porosity and well-coalesced grains reflect enhanced interfacial bonding, which can be attributed to the strong interaction between WC and the carbide matrix during SPS [10, 18]. The presence of WC likely imparts additional reinforcement, beneficial for hardness and wear resistance.

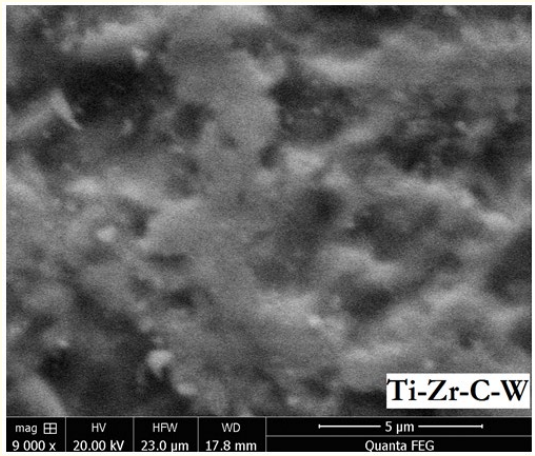

Figure 7: SEM image of the Ti-Zr-C-W composite at 9,000× magnification (5 μm scale bar), showing (Ti,Zr)C grains (1-2 μm) embedded with bright WC nanoparticles. The compact microstructure reflects enhanced cohesion and porosity suppression due to W doping.

These observations support the conclusion that dopant selection critically influences the final microstructure. While Mo enhances densification and grain refinement [15], W contributes to nanoparticle dispersion and improved cohesion [10, 16, 17, 18]. Both strategies improve the microstructural uniformity and integrity over undoped systems.

Parameter	***Ti-C***	***Zr-C***	***Ti-Zr-C***	***Ti-Zr-C-Mo***	***Ti-Zr-C-W Relative Density (%)***
Grain Size	1-2 μm	2-3 μm	1-4 μm	<1 μm	1-2 μm 98%
Homogeneity	Uniform	Heterogeneous	Phase separation (Ti/Zr-rich domains)	Highly homogeneous	Compact 94%
Porosity	Low	Moderate	Low	None	None 96%
Dopant Effect	-	-	Spinodal decomposition	Grain refinement (<1 μm)	WC nanoparticle dispersion >99%

Table 1: Comparative SEM Observations of Ti-C, Zr-C, Ti-Zr-C, Ti-Zr-C-Mo, and Ti-Zr-C-W Composites.

Compositional Insights from EDS Analysis

Energy-dispersive X-ray spectroscopy (EDS) provided elemental insight into the composition of the investigated composites (Table 2). The binary systems Ti-C and Zr-C showed near-stoichiometric elemental distributions, with Ti and Zr contents in the range of 65-75 at.% and 60-70 at.%, respectively, complemented by carbon at 25-35 at.% and 30-40 at.% [2]. Minimal oxygen contamination (<3 at.%) in both cases confirms successful processing under low-oxidation conditions, essential for carbide purity and performance.

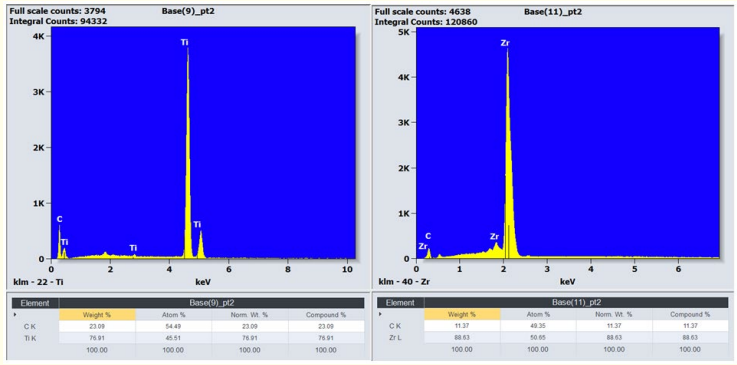

Figure 8: EDS spectra of Ti-C (left) and Zr-C (right) composites. The Ti-C spectrum shows strong titanium and carbon peaks with near-stoichiometric proportions and minimal oxygen contamination. The Zr-C spectrum confirms the presence of high-purity zirconium carbide with dominant Zr and C signals, also with low oxygen content (<2 at.%). Both spectra validate the successful synthesis of binary carbide phases.

The ternary Ti-Zr-C system showed a balanced elemental distribution with Ti (40-50 at.%), Zr (30-40 at.%), and C (20-30 at.%), consistent with the (Ti,Zr)C solid solution observed in SEM [12, 20]. The phase separation noted earlier is reflected in this dual-metal composition and indicates partial miscibility between TiC and ZrC domains under the applied SPS parameters [14].

In the Ti-Zr-C-Mo sample, molybdenum was detected at 5-10 at.%, evenly distributed throughout the matrix [15]. Its presence is likely associated with the formation of either solid-solution phases or secondary carbides such as Mo_2C. The ultrafine grain structure observed by SEM supports Mo's role as a grain refiner and sintering activator, facilitating densification without compromising chemical homogeneity.

The Ti-Zr-C-W composite contained tungsten at concentrations of 5-15 at.%, also uniformly dispersed [10, 16, 17]. The increased carbon content (25-35 at.%) suggests WC formation, which is in agreement with the bright nanoparticulate features identified in SEM images [16, 17, 18]. These WC inclusions likely serve as in-situ reinforcements that enhance hardness and suppress grain coarsening.

Overall, both Mo and W doping strategies were successful in integrating additional phases or modifying the matrix in ways that complement the microstructural goals—grain size control in the case of Mo [15], and nanoparticle reinforcement in the case of W [10, 16, 17, 18].

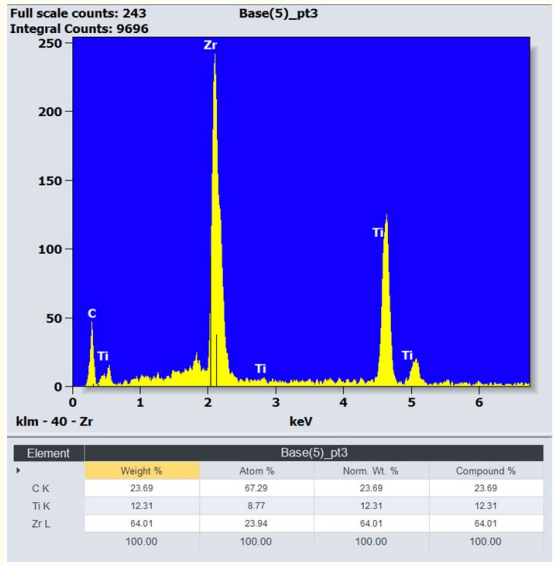

Element	Base(5)_pt3			
	Weight %	Atom %	Norm. Wt. %	Compound %
C K	23.69	67.29	23.69	23.69
Ti K	12.31	8.77	12.31	12.31
Zr L	64.01	23.94	64.01	64.01
	100.00	100.00	100.00	100.00

Figure 9: EDS spectrum of the Ti-Zr-C composite. The spectrum shows the presence of titanium, zirconium, and carbon, consistent with the formation of a (Ti,Zr)C solid solution. The elemental distribution supports the observed phase separation into Ti-rich and Zr-rich domains, as seen in SEM, with minimal oxygen contamination (<2 at.%).

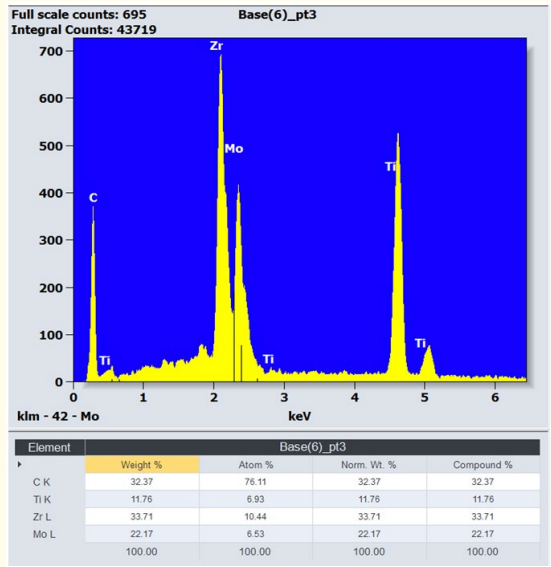

Element	Base(6)_pt3			
	Weight %	Atom %	Norm. Wt. %	Compound %
C K	32.37	76.11	32.37	32.37
Ti K	11.76	6.93	11.76	11.76
Zr L	33.71	10.44	33.71	33.71
Mo L	22.17	6.53	22.17	22.17
	100.00	100.00	100.00	100.00

Figure 10: EDS spectrum of the Ti-Zr-C-Mo composite indicating a uniform distribution of Mo (5-10 at.%) alongside Ti, Zr, and C, consistent with the formation of Mo-containing carbide phases and refined microstructure.

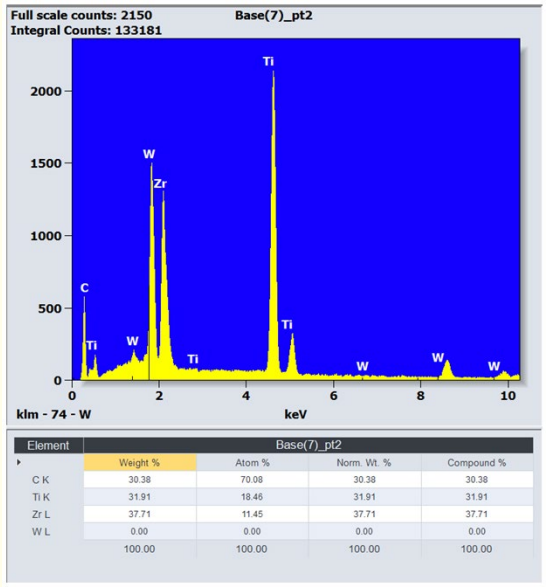

Figure 11: EDS spectrum of the Ti-Zr-C-W composite revealing tungsten incorporation (5-15 at.%) and elevated carbon levels, indicative of WC nanoparticle formation and matrix reinforcement.

Composite	*Major Elements (at.%)*	*Dopant/Additive*	*Notable Features*
Zr-C	Zr (60-70), C (30-40)	-	High-purity ZrC
Ti-C	Ti (65-75), C (25-35)	-	Stoichiometric TiC
Ti-Zr-C	Ti (40-50), Zr (30-40), C (20-30)	-	Phase-separated (Ti,Zr)C solid solution
Ti-Zr-C-Mo	Ti (35-45), Zr (25-35), C (20-30), Mo (5-10)	Mo	Mo-carbide formation, grain refinement
Ti-Zr-C-W	Ti (30-40), Zr (20-30), C (25-35), W (5-15)	W	WC dispersion, enhanced matrix cohesion

Table 2: Comparative EDS Results for Ti-C, Zr-C, Ti-Zr-C, Ti-Zr-C-Mo, and Ti-Zr-C-W Composites.

Mechanical Implications

The crack deflection in the Ti-Zr-C composite results from phase contrast between Ti-rich and Zr-rich domains, improving toughness [12, 20].

The combined SEM and EDS analyses provide a foundation for tailoring the mechanical properties of carbide composites. Mo-doped systems, with ultrafine grains and homogeneous structure, are ideal candidates for applications requiring high fracture toughness, such as advanced cutting tools [15, 10]. Conversely, W-doped systems exhibit features—such as WC reinforcement and dense interfacial bonding—that suggest superior hardness and wear resistance, making them suitable for armor and ballistic protection [16, 17, 18].

The undoped Ti-Zr-C composite, while structurally less refined, still offers potential due to its crack-deflection-promoting phase separation [20, 21, 22]. However, further optimization is required to reduce grain size variability and improve matrix cohesion. These comparative insights underscore the critical role of compositional engineering in achieving a balance of properties for high-performance carbide-based materials [9, 21, 23].

Conclusion

Mo additions enable ultrafine grain refinement and improved toughness, while W additions promote nanoparticle reinforcement and enhanced hardness. SPS processing proves highly effective in achieving dense, fine-grained carbide composites. These insights pave the way for the design of next-generation impact-resistant ceramic materials.

The incorporation of Mo into the Ti-Zr-C system promoted submicron grain refinement (<1 μm) and full densification, attributed to Mo's role as a grain growth inhibitor and sintering activator. In contrast, W doping facilitated the in situ formation of WC nanoparticles within the carbide matrix, enhancing interfacial cohesion and hardness while maintaining a compact microstructure. Undoped Ti-Zr-C composites exhibited phase separation into Ti-rich and Zr-rich domains, beneficial for crack deflection but limited by grain size heterogeneity. Structural and compositional analyses (XRD, SEM, EDS) confirmed the formation of FCC carbide solid solutions, with minimal oxidation and controlled dopant integration.

These results highlight the complementary roles of Mo and W: Mo optimizes fracture toughness through ultrafine, homogeneous microstructures, while W enhances wear resistance via nanoparticle reinforcement. Such tunability positions Mo-doped composites as candidates for precision cutting tools and W-doped systems for ballistic protection, where hardness and impact resistance are critical.

The success of the SPS process in achieving high densification (>98%) and rapid fabrication further underscores its suitability for engineering advanced ceramic composites. Future work should explore synergistic multi-dopant systems, long-term stability under operational conditions, and scalability of the SPS parameters for industrial adoption. This study provides a foundational framework for designing next-generation carbide materials that transcend traditional performance trade-offs, addressing pressing needs in defense, manufacturing, and high-temperature technologies.

Author Declarations

Conflict of Interest Statement

The authors declare that they have no conflicts of interest related to this work.

Data Availability

The data that support the findings of this study are available upon simple request to the corresponding author.

Ethics Statement

This research does not involve human participants or animals and therefore does not require ethical approval.

Funding Statement

This research received no external funding.

References

1. Pierson HO. "Handbook of Refractory Carbides and Nitrides: Properties, Characteristics". Processing and Applications. William Andrew Publishing (1996).
2. W Yujin., et al. "Research Progress on Preparation and Properties of Zirconium Carbide Matrix Composites". China's Refractories (2015).

3. Der-Liang Yung., et al. "Reactive sintering of ZrC-TiC composites". Key Engineering Materials 527 (2013): 20-25.
4. I Hussainova., et al. "ZrC-TiC-MoSi2 ceramic composite by spark plasma sintering". J. Phys.: Conf. Ser 1527 (2020): 012028.
5. Yanni Wei., et al. "Microstructure and mechanical properties of tungsten matrix composites synergistically reinforced with TiC-ZrC particles prepared by spark plasma". International Journal of Refractory Metals and Hard Materials 123 (2024): 106786.
6. Shi-Lei Li., et al. "Precise control of oxygen for titanium-zirconium-molybdenum alloy". International Journal of Refractory Metals and Hard Materials 103 (2022): 105768.
7. Demirskyi D., et al. "High-temperature toughening in ternary medium-entropy (Ta1/3Ti1/3Zr1/3)C carbide consolidated using spark-plasma sintering". Journal of Asian Ceramic Societies 8.4 (2020): 1262-1270.
8. XQ Xia., et al. "VC/NbC Content Effects on the Microstructure and Performance of Ti-Containing Tungsten-Cobalt Cemented Carbide". Strength of Materials 54 (2022): 127-133.
9. Divya Rana and Kantesh Balani. "Isolating strengthening contributions in multiphase high entropy (Zr-Ta-W-Ti)C-SiC based carbide ceramics". International Journal of Refractory Metals and Hard Materials 110 (2023): 106024.
10. Orrù R., et al. "Consolidation/synthesis of materials by electric current activated/assisted sintering". Materials Science and Engineering: R: Reports 63.4-6 (2009): 127-287.
11. Ying Li, Hirokazu Katsui and Takashi Goto. "Spark plasma sintering of TiC-ZrC composites". Ceramics International (2015).
12. Ying Li, Hirokazu Katsui and Takashi Goto. "Effect of heat treatment on the decomposition of TiC-ZrC solid solutions by spark plasma sintering". Journal of the European Ceramic Society (2016).
13. Lixia Xi, Lili Feng and Jürgen Eckert. "ZrC+TiC synergically reinforced metal matrix composites with micro/nanoscale reinforcements prepared by laser powder bed fusion". Journal of Materials Research and Technology (2022).
14. Ahram Moon, Chang-Yul Suh and Hanjung Kwon. "Fabrication of TiC-ZrC-Co composites with refined microstructure using ultrafine TiC-ZrC mixture powders". Journal of Alloys and Compounds (2018).
15. Zelin Luo, Yong Du and Zi-kui Liu. "Phase field simulation of the lamellar precipitation in the TiC-ZrC system". Ceramics International (2018).
16. Shaocun Liu, Wentao Hu and Zhongyuan Liu. "Mechanical properties of nanocrystalline TiC-ZrC solid solutions fabricated by spark plasma sintering". Ceramics International (2014).
17. Zelin Luo, Yong Du and Zikui Liu. "Phase field simulation of the phase separation in the TiC-ZrC-WC system". Calphad (2018).
18. Xiaobo Zhang, Ning Liu and Chunlan Rong. "Microstructure and fracture toughness of TiC-ZrC-WC-Mo-Ni cermets". International Journal of Refractory Metals and Hard Materials (2008).
19. Dong Wang., et al. "Microstructure and mechanical properties of intragranular W-Cu/TiC-ZrC composite prepared by reactive melt infiltration at 1300 °C". Materials Characterization (2018).
20. Xiaobo Zhang and Ning Liu. "Effects of ZrC on microstructure, mechanical properties and thermal shock resistance of TiC-ZrC-Co-Ni cermets". Materials Science and Engineering: A (2013).
21. Min-Soo Nam, Jae-Hyeong Choi and Seongwon Kim. "In-situ fabrication and characterization of W-ZrC composites via pressureless reaction sintering". International Journal of Refractory Metals and Hard Materials (2024).
22. M Sribalaji, Biswajyoti Mukherjee and Anup Kumar Keshri. "Microstructural and mechanical behavior of spark plasma sintered titanium carbide with hybrid reinforcement of tungsten carbide and carbon nanotubes". Materials Science and Engineering: A (2017).
23. Lei Su, Tianyu Xu and Libo Wang. "Study on the effect of ZrC and CNTs particles on Inconel 625 coatings fabricated by coaxial-wire-feed laser cladding". Journal of Materials Research and Technology (2024).